ACS OMEGA

http://pubs.acs.org/journal/acsodf

Article

Metabolic Reprogramming of the Right Ventricle and Pulmonary Arteries in a Flow-Associated Pulmonary Arterial Hypertension Rat Model

Dongli Liu, Suyuan Qin, Danyan Su, Kai Wang, Yanyun Huang, Yuqin Huang, and Yusheng Pang*

Cite This: *ACS Omega* 2022, 7, 1273−1287

Read Online

ACCESS | Metrics & More | Article Recommendations | Supporting Information

ABSTRACT: Pulmonary arterial hypertension (PAH) is a complex devastating disease relevant to remarkable metabolic dysregulation. Although various research studies on PAH from a metabolic perspective have been emerging, pathogenesis of PAH varies in different categories. Research on metabolic reprogramming in flow-associated PAH remains insufficient. An untargeted metabolomic profiling platform was used to evaluate the metabolic profile of pulmonary arteries (PAs) as well as the right ventricle (RV) in a flow-associated PAH rat model in the present work. A total of 79 PAs and 128 RV metabolites were significantly altered in PAH rats, among which 39 metabolites were assessed as shared dysregulated metabolites in PAs and the RV. Pathway analysis elucidated that, in PAs of PAH rats, pathways of phenylalanine, tyrosine, and tryptophan biosynthesis and linoleic acid metabolism were significantly altered, while in the RV, arginine biosynthesis and linoleic acid metabolism were altered dramatically. Further integrated analysis of shared dysregulated PA and RV metabolites demonstrated that the linoleic acid metabolism and the arachidonic acid (AA) metabolism were the key pathways involved in the pathogenesis of flow-associated PAH. Results obtained from the present work indicate that the PAH pathogenesis could be mediated by widespread metabolic reprogramming. In particular, the dysregulation of AA metabolism may considerably contribute to the development of high blood flow-associated PAH.

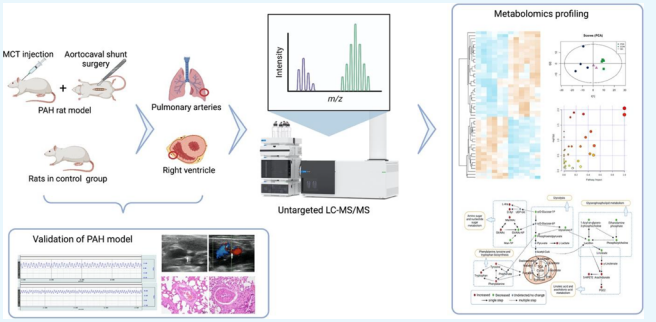

INTRODUCTION

Pulmonary arterial hypertension (PAH), primarily featured by elevated pulmonary arterial pressure (PAP) and remodeled and obstructed pulmonary vessels, is a complex and refractory lung disease.[1] The progressive increase in PAP will ultimately result in right ventricular hypertrophy (RVH) followed by cardiac dysfunction and even death. Survival of PAH patients is strongly associated with the right ventricular function.[2] Various factors contribute to PAH. Due to the intricate pathogenesis, although with greatly improved knowledge of treatment, the mortality of PAH is still high, making it a life-threatening disease.[3]

PAH is growingly regarded as a systemic disorder that is related to metabolic reprogramming and metabolic abnormality. Previous studies have reported that cancer-like metabolic features were observed in PAH patients' lungs, including shifted glucose metabolism (from relying on oxidative phosphorylation to dominant in aerobic glycolysis) as well as mitochondrial dysfunction.[4,5] Disturbance of the tricarboxylic acid (TCA) cycle,[6] fatty acid oxidation, and urea cycle,[7] as well as involvement of insulin resistance,[8] in the development of PAH has also been demonstrated by previous research. In parallel with increased resistance of pulmonary vessels, metabolic adaptations in the heart occur to improve the right ventricle (RV) function. Thus, glycolysis and fatty acid oxidation (FAO) were ultimately affected, and metabolic shifts similar to those found in the PAH lung tissue were developed in RV myocytes.[9,10] In light of these results, a theory that pulmonary vascular cells and extrapulmonary tissues share common metabolic abnormalities has been proposed by some authors.[11,12]

As the final downstream products of gene transcription, endogenous metabolites (such as peptides, amino acids, lipids, and nucleotides) present functional phenotypes of organisms or cells.[13] Metabonomics provides a comprehensive view of endogenous metabolites' alterations in the biological system in response to specific genetic modifications and pathophysiological stimuli.[14] With superior high sensitivity and specificity, liquid chromatography−tandem mass spectrometry (LC−MS/MS) is able to detect tiny variations in the intensity of metabolites and thus is widely being used in metabonomics

Received: October 21, 2021
Accepted: December 13, 2021
Published: December 27, 2021

© 2021 The Authors. Published by American Chemical Society

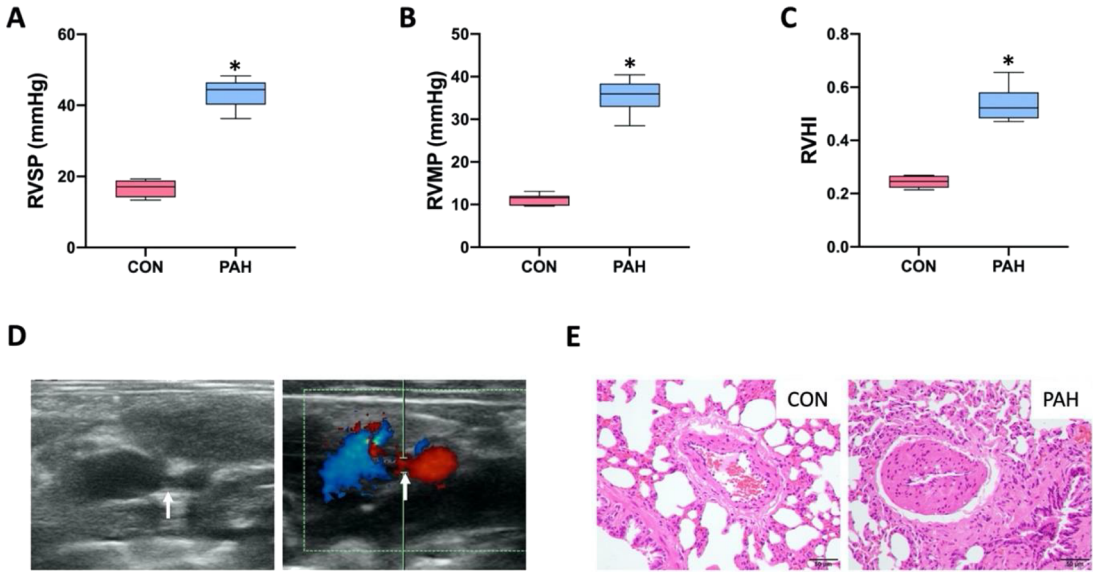

Figure 1. Pulmonary arterial hypertension (PAH) developed after fistulation operation. Compared to the control (CON) group, the right ventricular systolic pressure (RVSP) (A), right ventricular mean pressure (RVMP) (B), and right ventricular hypertrophy index (RVHI) (C) were considerably elevated in the PAH group (PAH, $n = 7$; CON, $n = 8$). (D) The fistulous tract and blood shunting between the inferior vena cava and the abdominal aorta were confirmed by two-dimensional ultrasonography (left) and color Doppler flow imaging (right) (the white arrows pointing toward the fistula). (E) HE staining showed a thickened pulmonary vessel wall, stenosis or a nearly occluded pulmonary arterial lumen, and perivascular inflammatory infiltrates in the PAH group. Data presented in graphs are means ± SD. *$P < 0.001$ versus CON. Scale bar, 50 μm.

research.[15] By using LC−MS, metabolomics analysis was conducted in previous studies to explore the metabolic abnormalities in the lung tissue[5] or the RV tissue of PAH.[16] However, the pathogenesis of PAH varies in different categories. The metabolic profiling in flow-associated PAH as well as shared metabolic abnormalities in the lungs and the RV is yet to be studied in detail.

In the current study, metabolic profiles of pulmonary arteries (PAs) and the RV in a flow-associated PAH rat model were identified via an untargeted metabolomics strategy. Shared metabolic abnormalities and metabolic pathways in PAs and the RV were analyzed. Thus, the metabolite signatures that might participate in the development of flow-associated PAH were characterized, which will probably contribute to developing a thorough insight into the pathophysiological mechanisms of PAH and reveal promising therapeutic targets for this devastating disease.

RESULTS

Validation of the PAH Model. Except one rat from the PAH group that died of overbleeding during hemodynamic measurement, the remaining animals were sacrificed after measurement. After monocrotaline (MCT) injection and abdominal aorta−inferior vena cava shunting surgery, hemodynamic measurement indicated a dramatic increase in right ventricular systolic pressure (RVSP) and right ventricular mean pressure (RVMP) in our flow-associated PAH model (Figure 1A,B). In accordance with increased RVSP and RVMP, rats in the PAH group showed obvious RVH, evidenced by the RVH index (RVHI) (Figure 1C). The fistulous tract between the inferior vena cava (IVC) and the abdominal aorta, and the multicolored blood flow signal of the shunt from the abdominal aorta to the IVC, was determined by two-dimensional and color Doppler ultrasonography (Figure 1D). Histological assessment of hematoxylin−eosin (HE) staining revealed that severe pulmonary vascular remodeling was presented in PAH rats. A thickened pulmonary artery intima−media, a narrowed or completely occluded pulmonary arterial lumen, and perivascular inflammatory infiltrates were visible in PAH rats (Figure 1E). Gomori aldehyde fuchsin (GAF) staining and Masson's trichrome staining revealed that the lungs of rats in the PAH group presented thickened intimal and medial pulmonary arteries (evidenced by pulmonary artery media thickness (PAMT)) (Figure 2A,B), with increased levels of collagen deposition, especially in the areas surrounding the vessels (Figure 2C,D). Moreover, cardiac fibrosis was exhibited in rats with PAH, as visualized by Masson's trichrome staining (Figure 2E,F). The successful establishment of the PAH model was verified by the above results.

Quality Control of LC−MS/MS Analysis. Principal component analysis (PCA) was carried out on the basis of the metabolites' characteristics obtained from all experimental groups as well as quality control (QC) samples, to examine LC−MS/MS data for potential distinctions, outliers, and other patterns (Figure 3A−D). From the results of PCA analysis, a clear pattern of separation was demonstrated between the control and PAH groups. Afterward, the orthogonal partial least-squares discriminant analysis (OPLS-DA) model was constructed; then; the variable importance in the projection (VIP) value of each feature was calculated. A clear clustering pattern within each group and noticeable discrimination between the control and PAH were exhibited in OPLS-DA score plots (Figure S1A−D). Furthermore, good reliability was visible from the parameters of the OPLS-DA model (Table 1).

Identification of Differential PA Metabolites. According to the VIP value > 1.0 and the P-value < 0.1, 37 dysregulated PA metabolites have been detected in negative ion mode, while 48 metabolites have been recognized as differential PA metabolites in positive mode. In both ion modes, 35 PA metabolites were upregulated in the PAH group, while 44 PA metabolites were downregulated (Figure 4A). The significantly altered PA metabolites could be mainly catego-

https://doi.org/10.1021/acsomega.1c05895
ACS Omega 2022, 7, 1273−1287

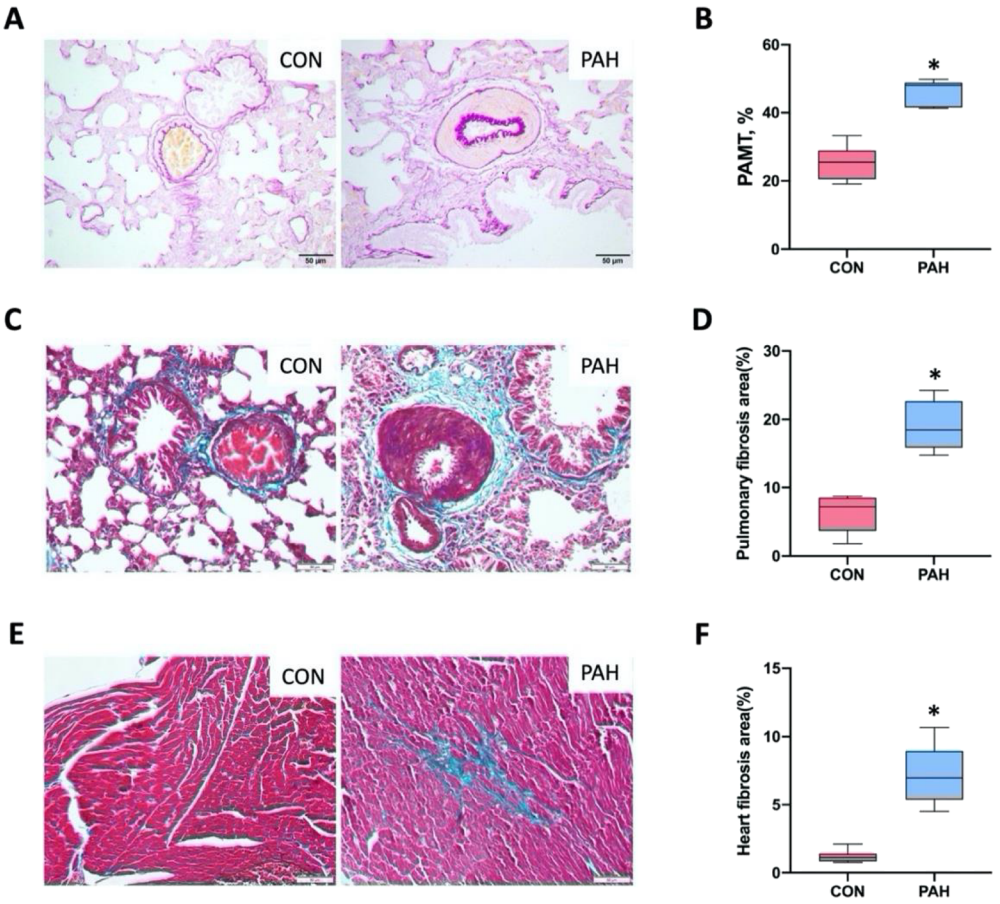

Figure 2. Pathologic characterizations of the lungs and the right ventricle (RV) of rats with PAH. (A) Representative images of gomori aldehyde fuchsin (GAF) staining of the lung tissue. The internal and external elastic fibers were stained purple. (B) Quantification of the pulmonary artery media thickness (PAMT) from GAF-stained sections. (C) Representative photographs of Masson's trichrome staining on lung sample slides. The collagen was stained green. (D) Quantification of the pulmonary fibrosis extent by using images of Masson's trichrome staining. (E) Masson's trichrome-stained sections of the RV were presented. (F) Quantification of the heart fibrosis area from Masson's trichrome-stained images. Data presented in graphs are means ± SD. *P < 0.001 versus CON (PAH, n = 7; CON, n = 8). Scale bar, 50 μm.

rized as carbohydrates, lipids, amino acids, carboxylic acids, vitamins, and others. Of note, carbohydrates, lipids, and amino acids account for more than half of all identified dysregulated metabolites (Figure 4B). Detailed information on these differential metabolites is provided in the Supporting Information (Table S1). The heat maps were constructed based on differential metabolites with the VIP value > 1.0 as well as the P-value < 0.05. As shown in heat maps (Figure 4D,E), the metabolic states of the PAH group have diverged significantly from the control group in both ion modes.

Identification of Differential RV Metabolites. According to the criteria VIP value > 1.0 and P-value < 0.1, 67 and 89 differential RV metabolites were obtained in the negative and positive ion modes, respectively. In both ion modes, 60 RV metabolites were upregulated in the PAH group, while 68 RV metabolites were downregulated (Figure 4A). The significant differential RV metabolites were mainly distributed as carbohydrates, amino acids, lipids, pyrimidines, purines, carboxylic acids, amines/amides, vitamins, and others, among which carbohydrates, amino acids, lipids, pyrimidines, and purines account for the majority (Figure 4C, detailed results are presented in Table S2). The heat maps were created based on differential metabolites with VIP > 1.0 (VIP score top 50) and P < 0.05. In both ion modes, heat map visualization (Figure 4F,G) of the top 50 differential metabolites presented distinct segregation between CON and PAH groups.

Biological Pathway Analysis of Dysregulated PA Metabolites. In order to recognize potential metabolic pathways associated with flow-associated PAH pathogenesis, dysregulated PA metabolites with the VIP value > 1.0 and the P-value < 0.1 were uploaded to MetaboAnalyst 5.0, a web tool that is based on the Kyoto Encyclopedia of Genes and Genomes (KEGG) metabolic pathway database and could provide visual statistical analysis (https://www.metaboanalyst.ca).[17−19] The dysregulated metabolic pathway was set as P < 0.05 as well as the pathway impact value > 0.1. Hence, five pathways were identified as dysregulated metabolic pathways, including phenylalanine, tyrosine, and tryptophan biosynthesis, linoleic acid metabolism, amino sugar and nucleotide sugar metabolism, glycerophospholipid metabolism, and glycolysis/gluconeogenesis (Figure 5A). Among these pathways, linoleic acid metabolism was significantly altered with the highest impact value, and the phenylalanine, tyrosine, and tryptophan biosynthesis pathway was also markedly altered with a high impact value together with the lowest P-value. It is worth noting that arachidonic acid (AA) metabolism may be a potential dysregulated metabolic pathway, as the P-value of this metabolic pathway is much close to 0.05 and with a high impact value. In Table S3 and Figures S2−S7, we summarized

https://doi.org/10.1021/acsomega.1c05895
ACS Omega 2022, 7, 1273−1287

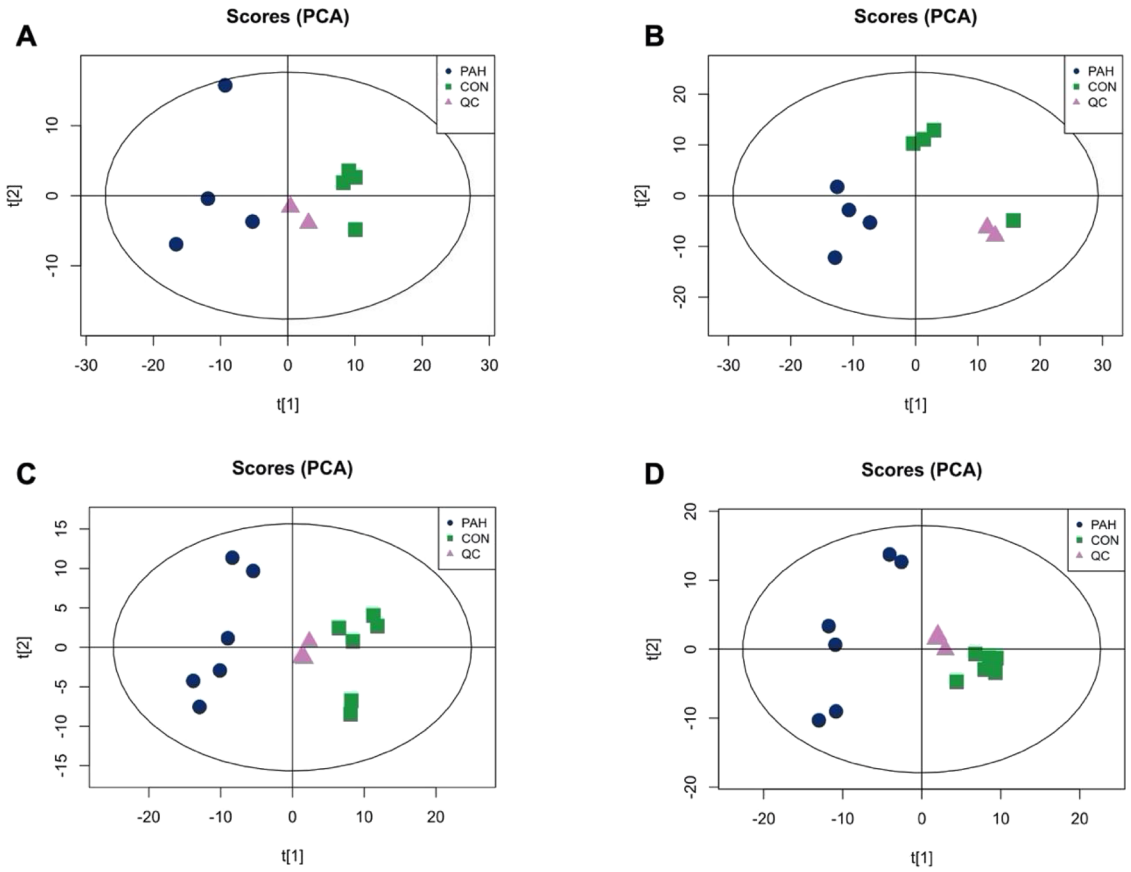

Figure 3. Principal component analysis (PCA) score maps based on metabolic profiles of pulmonary arteries (PAs) and the RV. (A,B) PCA score plots presented the degree of separation in metabolic profiles of PAs between CON and PAH groups in positive (A) and negative (B) ion modes. (C,D) The extent of separation of RV metabolic profiles in positive (C) and negative (D) ion modes is presented in PCA score plots. QC, quality control.

Table 1. Results of Permutation Tests for the OPLS-DA Model[a]

	ion mode	R^2Y	R^2X	Q^2
PAs	POS	1.000	0.733	0.901
	NEG	0.987	0.530	0.891
RV	POS	0.999	0.634	0.976
	NEG	0.996	0.580	0.951

[a]POS, positive; NEG, negative; PAs, pulmonary arteries; RV, right ventricle.

the differential metabolites participating in the above dysregulated metabolic pathways. In addition, on the basis of the KEGG database, dysregulated metabolic pathways and corresponding differential metabolites were presented by drawing united metabolic pathway networks (Figure 6).

KEGG Pathway Analysis of Dysregulated RV Metabolites. Obviously changed RV metabolites obtained from both ion modes were subjected to KEGG pathway analysis. Seven metabolic pathways were detected as dysregulated metabolic pathways, including amino sugar and nucleotide sugar metabolism, arginine biosynthesis, histidine metabolism, glycerophospholipid metabolism, pyrimidine metabolism, linoleic acid metabolism, and glycolysis/gluconeogenesis. Among these pathways, arginine biosynthesis and linoleic acid metabolism pathways were significantly disturbed with the lowest *P*-value and the highest pathway impact, respectively. Of note, D-glutamine and D-glutamate metabolism and purine metabolism pathways are potential dysregulated metabolic pathways, as D-glutamate and D-glutamine metabolism presents a high pathway impact with a *P*-value approaching 0.05, while purine metabolism displays a remarkable low *P*-value together with an impact value close to 0.1 (a graphical representation of disturbed pathways is displayed in Figure 5B, with detailed results listed in Table S4 and presented in Figures S8−S16). Based on KEGG pathway maps, the significant relevant metabolic pathways were shown by drawing united metabolic pathway networks together with corresponding differential metabolites (Figure 7). It is worth noting that all dysregulated metabolic pathways were associated with those related to energy metabolism such as glycolysis, nucleotide metabolism, and amino acid metabolism.

Integrated Analysis of Shared Differential Metabolites in PAs and the RV. Aiming to gain a deep insight into the mechanisms underlying the flow-associated PAH pathogenesis, integrated analysis of shared dysregulated metabolites in PAs and the RV was conducted. As presented in Figure 8A (Venn diagram) and in Table 2, between PAH and CON rats, there were 39 shared differential metabolites in the PAs and the RV. When classifying these shared dysregulated metabolites by their properties, the overwhelming majority was carbohydrates followed by lipids, purines/nucleosides, carboxylic acids, and amines (Figure 8B). Next, these shared dysregulated metabolites were subjected to KEGG pathway analysis, and five significantly dysregulated metabolic pathways were identified, including glycerophospholipid metabolism,

https://doi.org/10.1021/acsomega.1c05895
ACS Omega 2022, 7, 1273−1287

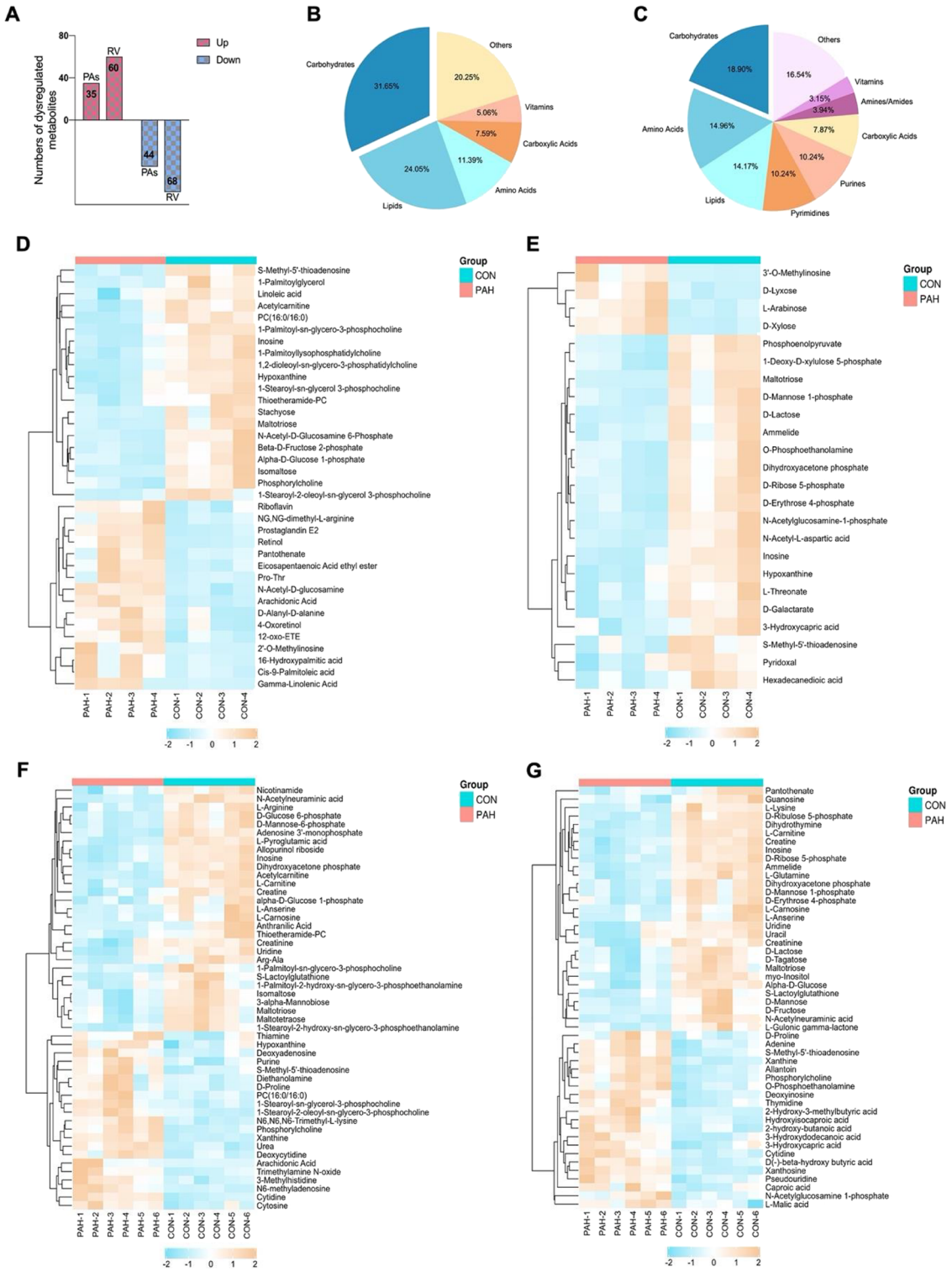

Figure 4. Heat maps visualizing the significantly altered metabolites between PAH and CON rats. (A) Numbers of increased and deceased PA and RV metabolites in PAH rats, (B) classification of dysregulated PA metabolites by their properties, (C) classification of dysregulated RV metabolites by their properties, (D,E) significantly altered metabolites in PAs, and (F,G) significant differential metabolites (the variable importance in the projection (VIP) score top 50 derived from OPLS-DA) in the RV. (D,F) Positive ion mode and (E,G) negative ion mode. Column: representing samples of each group; row: representing significantly dysregulated metabolites. The metabolite concentration was elucidated by the color key (lowest: blue; highest: orange).

glycolysis/gluconeogenesis, linoleic acid metabolism, AA metabolism, and amino sugar and nucleotide sugar metabolism (Figure 8C and Table 3). Among them, two pathways are relevant to carbohydrate metabolism, namely, the amino sugar and nucleotide sugar metabolism pathway and glycolysis/gluconeogenesis. Three of those five pathways were associated with lipid metabolism, including AA metabolism, linoleic acid metabolism, and glycerophospholipid metabolism. Notably,

https://doi.org/10.1021/acsomega.1c05895
ACS Omega 2022, 7, 1273−1287

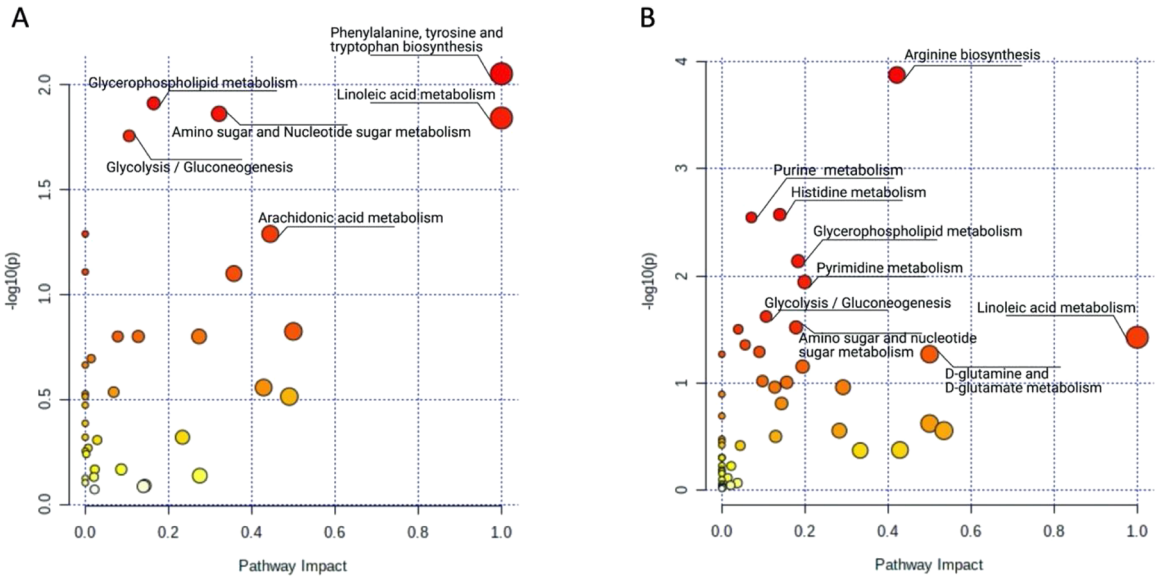

Figure 5. KEGG pathway analysis of dysregulated metabolites between CON and PAH rats. (A) KEGG pathway analysis of dysregulated metabolites (VIP value > 1 and *P*-value < 0.1) in PAs. (B) KEGG pathway analysis based on differential metabolites (VIP value > 1 and *P*-value < 0.1) obtained in the RV. The impact value derived from pathway topological analysis was presented by the size of the circles, and the magnitude of −log 10 (*p*-value) calculated through pathway analysis was represented by the color of the circles (lowest: light yellow; highest: dark red). Dysregulated metabolic pathways were labeled.

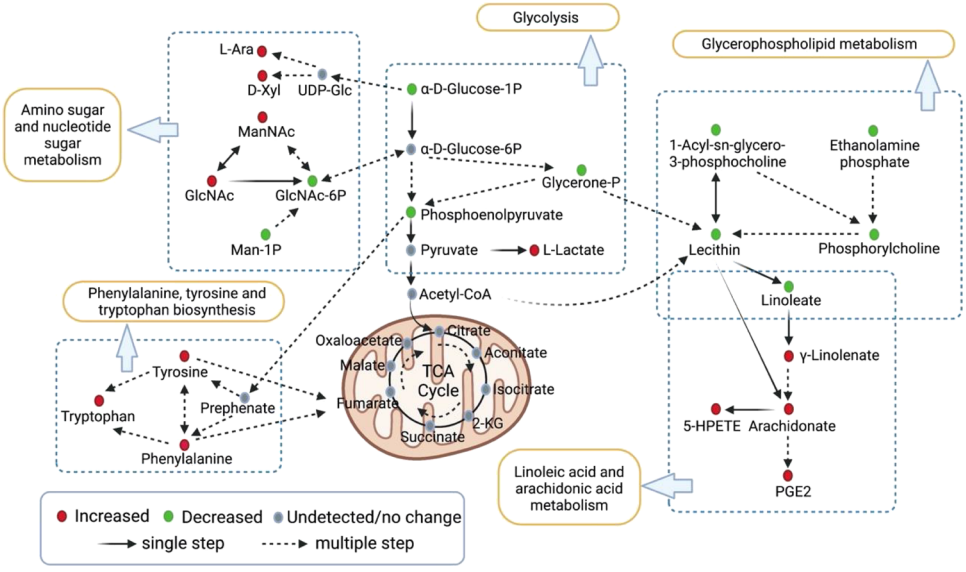

Figure 6. Schematic representation of significantly disturbed metabolic pathways in PAs of flow-associated PAH. Six dysregulated metabolic pathways in PAs of PAH rats were analyzed. Each circle represents a metabolite. Red and green ones represent that the metabolites were increased or decreased in PAs of PAH rats, respectively. Solid arrows represent single-step metabolism, while dashed arrows represent multiple-step metabolism. Dashed boxes indicate different metabolic pathways. α-D-Glucose-1P, α-D-glucose 1-phosphate; α-D-Glucose-6P, α-D-glucose 6-phosphate; Acetyl-CoA, acetyl coenzyme A; D-Xyl, D-xylose; GlcNAc-6P, *N*-acetyl-D-glucosamine 6-phosphate; GlcNAc, *N*-acetyl-D-glucosamine; Glycerone-P, dihydroxyacetone phosphate; L-Ara, L-arabinose; Man-1P, D-mannose 1-phosphate; ManNAc, *N*-acetyl-D-mannosamine; PGE2, prostaglandin E2; TCA, tricarboxylic acid; UDP-Glc, uridine diphosphate glucose; 2-KG, 2-ketoglutaric acid; 5-HPETE, 5-hydroperoxyeicosatetraenoic acid.

among these three pathways, AA metabolism and linoleic acid metabolism exhibited a high impact value, while glycerophospholipid metabolism showed the lowest *P*-value.

Figure 9 shows the disturbance of linoleic acid and AA metabolism and corresponding dysregulated metabolites in flow-associated PAH. It is well-known that linoleic acid and AA metabolism pathways play a pivotal role in inflammation.[20] The present study showed that some key metabolic intermediates or end products, which are related to linoleic acid and AA metabolism, presented a dramatic increase in rats with PAH, including γ-linolenic acid, AA, 5-hydroperoxyeicosatetraenoic acid (5-HPETE), and prostaglandin E2 (PGE2), while the substrate, linoleic acid, presented a significant decrease. Among these, linoleic acid, AA, and PGE2 are shared differential PA and RV metabolites in PAH. Synthesized from linoleic acid, AA is a long-chain fatty acid that could be converted into prostaglandin H2 (PGH2) by cyclooxygenases (COXs). PGH2 serves as the substrate for a series of enzymes,

https://doi.org/10.1021/acsomega.1c05895
ACS Omega 2022, 7, 1273−1287

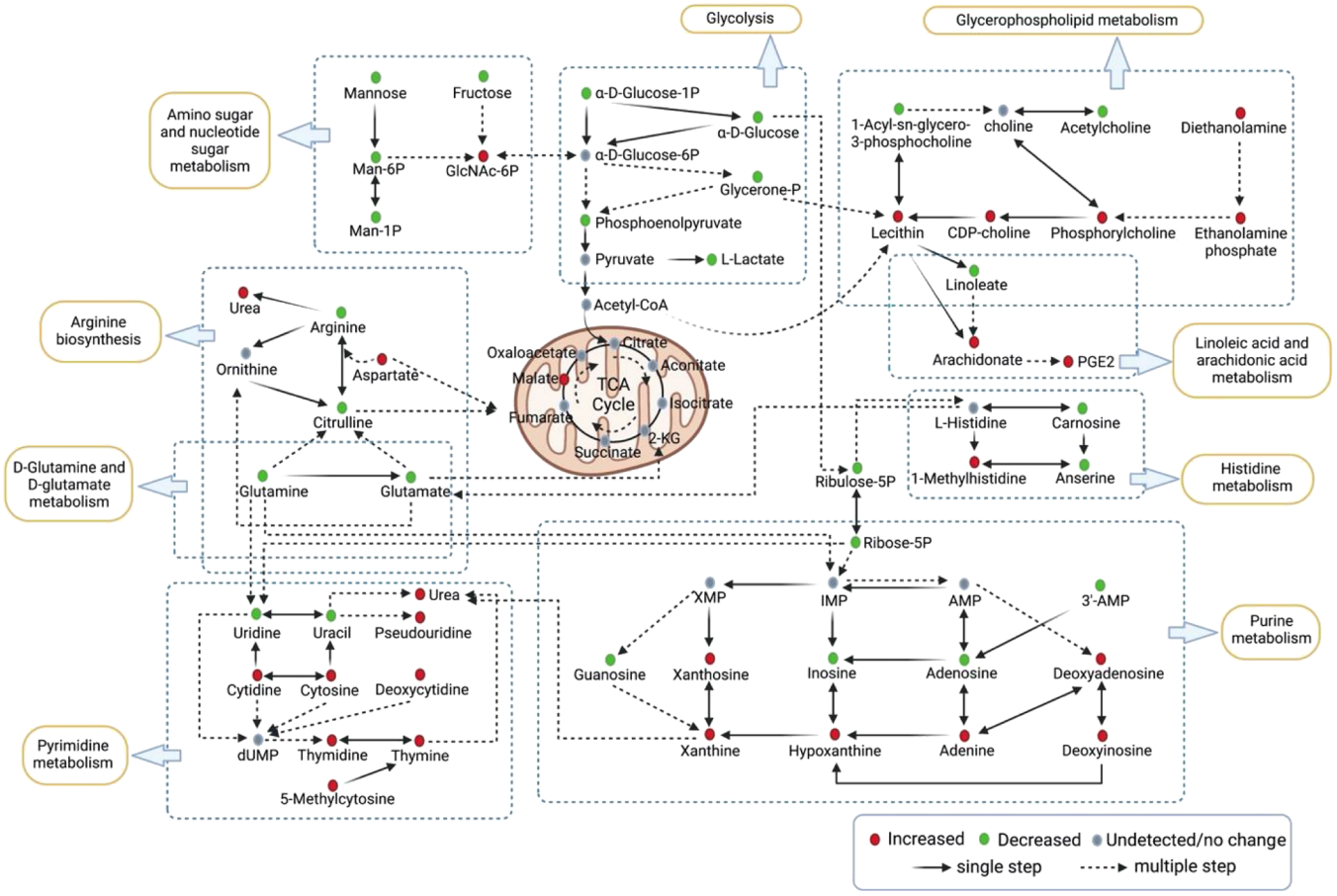

Figure 7. Schematic representation of significantly disturbed metabolic pathways in the RV of flow-associated PAH. Nine dysregulated metabolic pathways in the RV of PAH groups were analyzed. Each circle represents a metabolite. Red and green ones represent that the metabolites were increased or decreased in the RV of PAH groups, respectively. Solid arrows represent single-step metabolism, while dashed arrows represent multiple-step metabolism. Dashed boxes indicate different metabolic pathways. α-D-Glucose-1P, α-D-glucose 1-phosphate; α-D-Glucose-6P, α-D-glucose 6-phosphate; Acetyl-CoA, acetyl coenzyme A; AMP, adenosine 5′-monophosphate; CDP-choline, cytidine 5′-diphosphocholine; dUMP, deoxyuridine monophosphate; GlcNAc-6P, *N*-acetyl-D-glucosamine 6-phosphate; Glycerone-P, dihydroxyacetone phosphate; IMP, inosine 5′-monophosphate; Man-1P, D-mannose 1-phosphate; Man-6P, D-mannose 6-phosphate; PGE2, prostaglandin E2; Ribose-5P, D-ribose 5-phosphate; Ribulose-5P, D-ribulose 5-phosphate; TCA, tricarboxylic acid; XMP, xanthosine 5′-phosphate; 2-KG, 2-ketoglutaric acid; 3′-AMP, adenosine-3′-monophosphate.

each resulting in a different prostaglandin (PG) end product. Vascular smooth muscle cells mainly produce PGs, such as PGE2 and prostaglandin F2α (PGF2α). PGE2 exhibits a variety of biological activities, for instance, inflammation, cell proliferation, and antiapoptosis, via its receptors.[21] Unlike PGE2, PGF2α commonly acts as a vasoconstrictor. AA could also be metabolized by 5-lipoxygenase into 5-HPETE, which in turn is converted into different leukotrienes (LTs). Some LTs (such as C4, D4, and E4) are known to induce certain pathological hallmarks of PAH, including an increase in vascular permeability and pulmonary vasoconstriction.[22] Collectively, an inflammatory microenvironment, formed by LTs and PGs derived from AA, could serve as a stimulation and attraction factor of leukocytes, which makes AA a central regulator of the inflammatory response.[20] The findings from the current study suggest that the AA metabolism was remarkably promoted in PA and RV tissues in flow-associated PAH, which may considerably contribute to the onset of PAH.

DISCUSSION

In the present work, the metabolic profile of PAs and the RV in a high pulmonary flow-associated PAH animal model has been characterized through untargeted metabolomics. Moreover, integrated analysis was carried out to explore shared differential metabolites as well as dysregulated metabolic pathways in PAs and the RV. Metabolic reprogramming of PAH has been previously characterized in animal models[14,16,23,24] and patients.[25−28] It should be noted that most of these studies were designed to assess the metabolic profile in one particular tissue or sample, such as blood (plasma/serum), the lungs, or the RV tissue. Izquierdo-Garcia et al.[29] have used NMR-based metabolomics together with the technique of 18F-FDG PET imaging to characterize the metabolic profile in the heart and lung tissues in a PAH mouse model. However, the differential metabolites that they researched were limited, and the shared lung and heart dysregulated metabolites have not been comprehensively analyzed. A previous study reported that distinct animal models, for instance, hypoxia-induced and MCT-induced PAH, may develop PAH through different metabolomic pathways.[30] Currently, the available data on the metabolic shift in pulmonary overcirculation-associated PAH appear to be insufficient, thereby deserving to be studied deeply. As far as we are aware, for the first time, we evaluated PA and RV metabolic reprogramming as well as shared

https://doi.org/10.1021/acsomega.1c05895
ACS Omega 2022, 7, 1273−1287

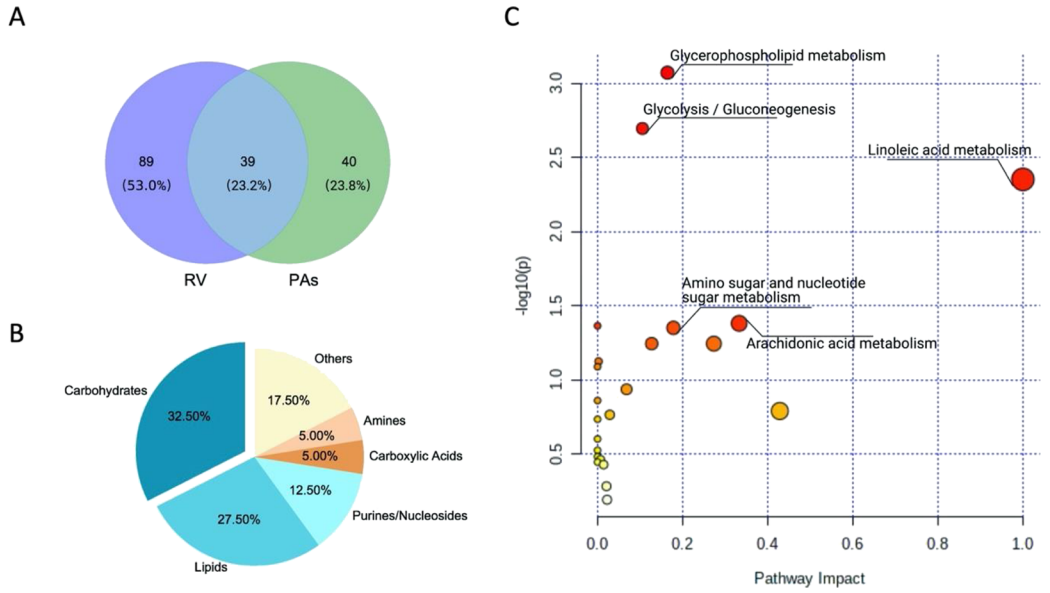

Figure 8. Integrated analysis of shared differential metabolites in PAs and the RV. (A) Venn diagram representing the comparison of differential metabolites between PAs and the RV. There are 39 shared differential metabolites between PAs and the RV. (B) Classification of 39 shared differential PA and RV metabolites by their properties. (C) KEGG pathway analysis based on the selected 39 shared differential metabolites after integration of both PA and RV metabolomics datasets. The importance of a metabolic pathway was elucidated by the size and color of the circle. Influenced metabolic pathways were labeled.

metabolic abnormalities in the flow-associated PAH. The current study brings insights into the metabolic feature of two important target organs (the lungs and the RV) for flow-associated PAH, with the possibility to develop novel therapeutic targets.

In patients with left−right flow shunt congenital heart disease (CHD), PAH usually develops progressively as a consequence of chronic pulmonary overcirculation. A representative animal model that could reproduce the pathological hallmarks of human CHD-associated PAH (CHD-PAH) is necessary for a deep understanding of the pathobiology of this devastating disease. A rodent model of flow-associated PAH that combines MCT injection and aortocaval shunt was applied in this work for its potential to double the volume of pulmonary flow and to induce the formation of a neointimal-type vascular remodeling, which is similar to PAH in mankind.[31] Moreover, it presents more pronounced right heart failure as well as increased morbidity and mortality.[31] Thus, it was considered to be an ideal flow-associated PAH model to mimic CHD-PAH[32] and could be employed to explore subtle metabolic disturbances specifically linked to the RV and pulmonary vascular remodeling. In the present work, the formation of the characteristics of PAH was clearly confirmed in our rat model through hemodynamic measurement and histological examination.

An expanding body of evidence has shed light on the important role of inflammation in PAH pathogenesis.[33,34] The presence of high levels of multiple chemokines and cytokines has been well confirmed in lung tissues of patients and animals with PAH. Disorder of pulmonary hemodynamics and remodeling of pulmonary vessels in PAH were closely correlated with the degree of perivascular inflammation.[35] The recruitment of inflammatory cells, for instance, neutrophils and monocytes, leads to dramatic changes in the metabolic activity of inflamed tissues. A notable metabolic disorder during inflammation involves the generation of lipid mediators.[36] AA, synthesized from linoleic acid, is a long-chain fatty acid that could be converted into LTs by lipoxygenase or into PGH2 by COXs. By binding to 4G protein-coupled receptors, PGE2, the downstream proinflammatory product of AA, could enable the activation of adenylate cyclase as well as numerous downstream signaling pathways, thereby promoting the expression levels of many inflammatory factors, such as TNF-α, IL-1, and IL-6.[37] Chen et al. reported that, compared with the healthy control, in serum samples of CHD-PAH, α-linolenic acid metabolism and AA metabolism were remarkably disturbed.[25] Consistently, in the present study, linoleic acid metabolism and AA metabolism pathways have been proven to be the most pivotal dysregulated pathways in PAs and the RV, evidenced by high impact values obtained in KEGG pathway analysis based on the selected 39 shared differential PA and RV metabolites. Specifically, a highly increased load of AA and PGE2 and a decreased level of linoleic acid were found in PAs and the RV of rats with PAH. An increased level of AA in plasma,[38] serum,[25] the lungs,[14,38] and the heart[38] of PAH patients[25] or animal models[14,38] has been reported by previous research, pointing out the potential role of AA in the onset and progress of PAH. The present study extended these findings by showing evidence of substrate depletion of AA metabolism (decrease in linoleic acid) and an increase in downstream products (such as PGE2 and 5-HPETE), robustly indicating that the AA metabolic pathway was significantly activated in PAH. Taking this together, we suggest that abnormalities in AA metabolism reflect a common signature correlated with an extensive inflammatory response in the lungs and the RV, which might play a critical role in the development of high pulmonary blood flow-associated PAH.

In this study, glycerophospholipid metabolism was found to be a shared dysregulated pathway in PAs and the RV of PAH. Glycerophospholipids, the most abundant phospholipids in the lungs, are pivotal for oxidative stress, lung defense, and the inflammatory response.[39,40] A previous study has demonstrated that downregulation of the glycerophospholipid metabolic pathway, observed in severe COPD, was significantly

https://doi.org/10.1021/acsomega.1c05895
ACS Omega 2022, 7, 1273−1287

Table 2. The Detailed Results of Shared Differential Metabolites in PAs and the RV[a]

metabolites	PAs			RV		
	VIP	FC	*p*-value	VIP	FC	*p*-value
Carbohydrates						
α-D-glucose 1-phosphate	2.798	0.296	0.008	2.782	0.662	0.004
D-erythrose 4-phosphate	1.170	0.296	0.002	1.526	0.679	0.002
D-galactarate	5.044	0.340	0.001	1.514	0.763	0.051
D-glucose 6-phosphate	2.961	0.344	0.074	3.470	0.622	1.8×10^{-4}
D-mannose-1-phosphate	7.760	0.195	0.011	8.600	0.608	1.9×10^{-4}
D-ribose	1.323	1.315	0.052	1.000	1.648	0.020
dihydroxyacetone phosphate	1.627	0.338	0.010	2.602	0.572	6.7×10^{-6}
maltotriose	2.404	0.523	0.005	5.229	0.508	0.004
N-acetylglucosamine 1-phosphate	2.302	0.438	0.002	1.882	1.404	0.031
N-acetyl-D-glucosamine 6-phosphate	1.212	0.400	0.003	1.010	1.346	0.056
N-acetylneuraminic acid	1.029	1.324	0.078	3.699	0.475	1.3×10^{-5}
stachyose	1.190	0.509	0.015	1.208	0.494	0.004
thioetheramide-PC	5.482	0.708	0.030	6.085	0.499	0.013
Lipids						
acetylcarnitine	10.950	0.816	0.015	9.125	0.518	4.4×10^{-7}
arachidonic acid	4.324	3.702	1.5×10^{-4}	4.485	8.757	0.049
hexadecanedioic acid	1.091	0.573	0.016	1.180	1.526	0.011
linoleic acid	2.830	0.700	0.032	2.037	0.737	0.010
PC(16:0/16:0)	4.728	0.520	0.001	2.409	2.902	0.015
prostaglandin E2	20.417	3.088	1.7×10^{-4}	2.054	3.575	0.001
1-palmitoyl-*sn*-glycero-3-phosphocholine	18.753	0.612	0.010	12.224	0.711	0.009
1-palmitoyl-2-hydroxy-*sn*-glycero-3-phosphoethanolamine	4.443	0.353	0.093	4.485	0.637	0.031
1-stearoyl-*sn*-glycerol-3-phosphocholine	16.226	0.569	0.015	16.822	2.444	0.004
3-hydroxycapric acid	1.179	0.350	0.029	1.365	1.516	0.007
Purines/nucleosides						
adenine	1.639	0.512	0.079	3.266	1.513	0.001
D-lyxose	5.517	2.012	0.004	1.039	0.572	0.034
hypoxanthine	19.498	0.634	0.006	2.510	1.195	0.015
inosine	4.040	0.361	0.001	21.974	0.679	4.8×10^{-6}
S-methyl-5′-thioadenosine	5.762	0.387	0.001	10.633	1.610	0.006
Carboxylic acids						
lactate	1.613	1.413	0.077	7.602	0.844	0.082
phosphoenolpyruvate	1.025	0.329	0.001	1.149	0.732	0.002
Amines						
O-phosphoethanolamine	1.284	0.348	0.010	1.222	1.359	0.003
phosphorylcholine	9.149	0.403	0.007	12.601	1.377	1.5×10^{-4}
Others						
ammelide	1.009	0.312	0.011	1.552	0.748	3.9×10^{-6}
D-lactose	2.129	0.445	0.002	1.607	0.510	0.001
D-ribose 5-phosphate	1.799	0.256	0.004	2.898	0.539	4.7×10^{-6}
isomaltose	2.687	0.482	0.003	5.547	0.517	0.001
N-acetyl-L-alanine	1.790	1.606	0.052	1.294	0.513	0.029
pantothenate	2.510	1.643	0.038	5.009	0.734	0.023
taurine	4.506	0.709	0.095	1.127	1.634	2.8×10^{-4}

[a]PAs, pulmonary arteries; RV, right ventricle; FC, fold change; VIP, variable importance in the projection.

Table 3. Pathway Analysis Based on the Selected 39 Shared Differential Metabolites in PAs and the RV

metabolic pathway	*P*-value	−log 10(p)	FDR[a]	impact
glycerophospholipid metabolism	0.001	3.071	0.071	0.164
glycolysis/gluconeogenesis	0.002	2.695	0.085	0.106
linoleic acid metabolism	0.004	2.351	0.125	1.000
arachidonic acid metabolism	0.042	1.380	0.599	0.333
amino sugar and nucleotide sugar metabolism	0.045	1.350	0.599	0.178

[a]FDR, false discovery rate.

negatively correlated with oxidative stress products.[39] In addition, the strong relationship between phosphatidylcholine and inflammatory factors in lung tissues in sepsis-induced acute lung injury was also reported by prior research.[41] During pulmonary vascular remodeling, an increase in oxidative stress has been corroborated in the lungs and pulmonary vasculature. Moreover, in an interactive manner, oxidative stress together with inflammation plays a crucial role in the development of pulmonary vascular remodeling.[42] Results from the current study presented that the PA metabolites such as phosphorylcholine, dihydroxyacetone phosphate, *O*-phosphoethanolamine, lecithin, and 1-palmitoyl-*sn*-glycero-3-phosphocholine

https://doi.org/10.1021/acsomega.1c05895
ACS Omega 2022, 7, 1273−1287

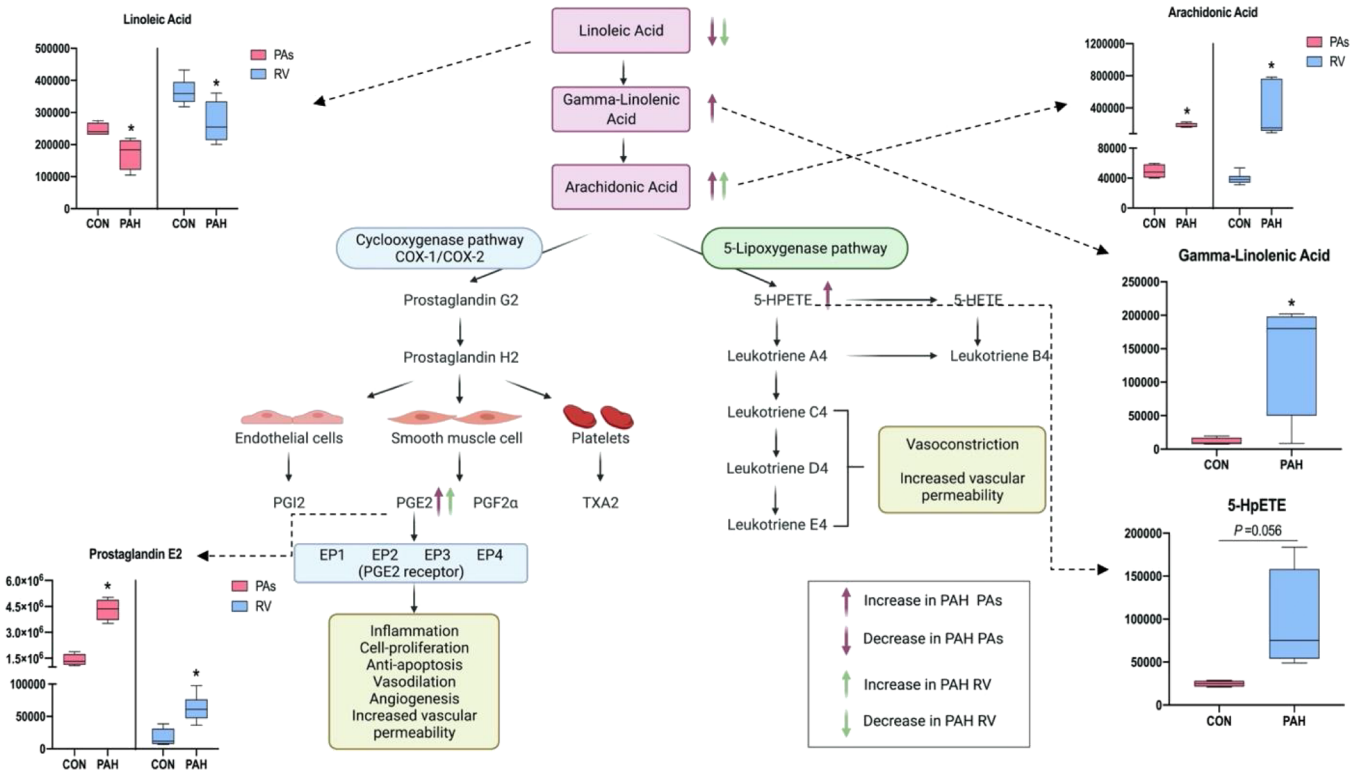

Figure 9. Disturbance of linoleic acid and arachidonic acid (AA) metabolism and corresponding dysregulated metabolites in flow-associated PAH. An overview of the metabolic flow of linoleic acid and AA metabolism and alterations identified in PAs and the RV between PAH and CON groups. Data presented in graphs are means ± SD. *P < 0.05 versus CON. PGE2, prostaglandin E2; EP, prostaglandin E2 receptor; PGF2α, prostaglandin F2α; PGI2, prostacyclin I2; TXA2, thromboxane A2; 5-HPETE, 5-hydroperoxyeicosatetraenoic acid.

were decreased in the PAH group, indicating downregulation of glycerophospholipid metabolism. Therefore, we speculated that downregulation of glycerophospholipid metabolism results in an increase in oxidative stress by regulating inflammatory response, thus acting as a key factor in pulmonary vascular remodeling and development of PAH. However, unlike the result in PAs, our data showed a relatively upregulated glycerophospholipid metabolism in RV samples of the PAH group, evidenced by the increased levels of phosphorylcholine, lecithin, *O*-phosphoethanolamine, diethanolamine, and cytidine 5′-diphosphocholine. It is widely accepted that during the development of heart failure, lipid accumulation in cardiomyocytes serves as one of the causal factors.[43] Glycerophospholipids, a lipid class, were reported to act as a predominant bioactive contributor bridging insulin resistance and cardiac damage.[44] PC(16:0/16:0), an intermediate of glycerophospholipid metabolism, which presented a 2.9-fold increase in the RV of PAH rats in our study (Table S2), was also found to be upregulated in rats with doxorubicin-induced chronic heart failure.[45] Therefore, we speculated that the increase in products of glycerophospholipid metabolism may be cardiac lipotoxic and has potential adverse effects on the cardiac function. However, given limited evidence, the role of glycerophospholipid metabolism in pulmonary vascular and right ventricular remodeling in PAH requires future studies to elucidate.

When classifying dysregulated PA and RV metabolites by their properties, carbohydrates (including glucose, amino sugar, nucleotide sugar, and so on) accounted for the majority of all identified dysregulated metabolites. As an important energy source of pulmonary smooth muscle cells (PASMCs) and cardiomyocytes, dramatically disturbed carbohydrates indicate a robust imbalance in energy metabolism. These disturbed carbohydrate metabolisms found in our study include amino sugar and nucleotide sugar metabolism as well as glucose metabolism (glycolysis/gluconeogenesis). It is generally considered that there is a glycolytic shift in PASMCs and the RV during the development of PAH, with increased glycolysis and decreased glucose oxidation.[11] Consistent with previous studies, the detection of significant decreases in glycolytic substrates (α-D-glucose 1-phosphate and phosphoenolpyruvate) and accumulation of end products (lactate) in PAs of PAH rats in our study strongly suggested the alteration in glycolytic metabolism. However, no evidence of relatively increased glycolysis was present in the RV of PAH rats in our present work. Our results suggested relatively reduced glycolysis in the RV of PAH rats compared to the control. Of note, it has been reported in previous studies that in the RV tissue of hypoxia-induced PAH, substrates and products of glycolysis could be maintained at a nearly normal level.[24,46] In addition, interestingly, unlike increased glycolysis showing in early or developing PAH in several previous studies, reduced glycolysis was observed in human lungs with advanced PAH.[5] A possible interpretation of these contradictory results may be that the metabolic dysregulation in the RV is probably driven by intrinsic changes at the level of cardiomyocytes that were triggered by an increased afterload, rather than a consequence induced by imbalance between energetic demands and uptake of oxygen. Thus, cardiomyocytes display heterogeneous phenotypes in distinct stages during the development of the disease. The role of amino sugar and nucleotide sugar metabolism in PAH remains unclear. It has been reported

https://doi.org/10.1021/acsomega.1c05895
ACS Omega 2022, 7, 1273−1287

that amino sugar and nucleotide sugar metabolism is related to the disturbance of redox homeostasis. Disturbance of amino sugar and nucleotide sugar metabolism was found in hypertrophic cardiomyopathy[47] and asthma, a chronic inflammatory airway disease with the characteristic of airway remodeling.[48] *N*-acetyl-D-glucosamine 6-phosphate, an intermediate metabolite of amino sugar and nucleotide sugar metabolism, which was dysregulated both in PAs and the RV in our PAH model, was identified as a potential biomarker for the diagnosis of coronary heart disease (a kind of cardiovascular disease that was thought to undergo a metabolic shift).[49] Taken together, our results suggested that the perturbation of energy metabolism was involved in the development of flow-associated PAH, especially the carbohydrate metabolism.

Accumulating evidence has revealed the key role of amino acids in the pathogenesis of PAH.[25,50] In our study, compared with the CON group, phenylalanine, tyrosine, and tryptophan biosynthesis was the most significantly dysregulated metabolic pathway in PAs of the PAH group, while arginine biosynthesis and histidine metabolism are two significantly disturbed pathways in the RV. These pathways are all relevant to amino acid metabolism. Phenylalanine, when substantially increased, is recognized to be involved in numerous pathophysiological processes, such as chronic obstructive pulmonary disease,[51] persistent pulmonary hypertension,[52] and coronary heart disease.[53] Tan et al. demonstrated that chronic phenylalanine administration induced PAH through binding to the calcium-sensing receptor and its subsequent activation in rats.[54] According to this finding, they proposed a hypothesis that phenylalanine probably accumulates in the lungs of PAH, which was not previously reported but was confirmed by our current work. Furthermore, tryptophan, an essential amino acid that could act as a precursor in serotonin production, was found to be upregulated in PAH PAs in our study. Synthesized in the pulmonary endothelium, serotonin could pass into the underlying PASMCs to trigger the overproliferation and contraction response of PASMCs. Moreover, serotonin could also participate in mediating the proliferation of fibroblasts in the lungs.[55] Given these, although the influence of tryptophan in PAH remains poorly understood, one reasonable hypothesis is that it possibly involves the development of this disease through the serotonergic pathway.[56] According to World Health Organization guidelines, tryptophan has been categorized as a likely causative agent for the development of PAH.[57] In normal cases, FAO in the mitochondria of cardiomyocytes serves as a primary source of energy supply. In patients with cardiac dysfunction, a remarkable shift from relying on FAO to preferential utilization of alternative sources of energy was observed.[43] In this condition, on account of hormonal imbalance, coenzyme depletion, and inflammatory activation, carbohydrate metabolism is inefficient; thus, amino acids are essential for the TCA cycle.[58] Noteworthy, we found noticeable decreases in the RV content of L-glutamine and L-glutamate, two metabolites that could serve as a carbon source for energy production, replenishing the TCA cycle.[46] In addition, in the RV of PAH rats, decreases in arginine biosynthesis and histidine metabolism were detected, evidenced by the substantial decrease in arginine, citrulline, carnosine, and anserine. We propose that the decrease in these amino acids' concentration was probably due to their increased utilization by the mitochondria to fuel the TCA cycle, thereby increasing the generation of ATP as well as maintaining the function of the mitochondria. This could be partly supported by a previous study, which reported that in glioblastoma lines, glutamine was used as an alternative carbon source to provide a steady source of oxaloacetate and maintain back half flow through the TCA cycle.[59] On the other hand, as nitric oxide precursors, citrulline and arginine present a cardioprotective function.[60] It has been demonstrated that plasma levels of arginine and citrulline dropped precipitously after congenital cardiac surgery,[61] while citrulline and arginine supplementation played a protective role in PAH.[60,61] Furthermore, in patients with preserved ejection fraction heart failure, administration of arginine and citrulline contributed to an improvement in pulmonary vascular resistance as well as the right ventricular ejection fraction, thereby improving the right ventricular function.[62] Collectively, the decreased level of these amino acids may be hallmarks of a dysregulated RV function in PAH.

Pyrimidine metabolism and purine metabolism belong to nucleotide metabolism, which is a key pathway that generates pyrimidine and purine molecules for DNA synthesis and replication. It has been demonstrated that plasma levels of purine metabolites (such as xanthine, xanthosine, uric acid, and so forth) were upregulated in PAH, indicating increased oxidative stress. Moreover, plasma levels of purine metabolites were reported to be related to the severity of PAH and RV dysfunction.[63] In our present study, pyrimidine and purine metabolism was found to be upregulated in the RV of PAH rats since relevant metabolites including adenine, xanthosine, xanthine, hypoxanthine, deoxyadenosine, deoxyinosine, cytidine, cytosine, deoxycytidine, pseudouridine, thymidine, thymine, and 5-methylcytosine were significantly increased. A previous study reported that an elevated pyrimidine metabolite content (such as pseudouridine and orotic acid) as well as increased purine metabolites (for instance, inosine, hypoxanthine, and uric acid) were correlated with cardiotoxicity of anthracyclines.[64] Although these metabolic pathways have not been sufficiently reported in PAH, our study suggested that they are prominent pathways relevant to PAH pathogenesis and may be potential targets for further mechanistic research.

CONCLUSIONS

PAH, a rare but lethal disease, has been increasingly recognized as a systemic disorder characterized by metabolic derangements.[65,66] Since the lungs are the primary target organ of PAH, the pathological alteration in PAs has been the traditional subject of most of the intensive research studies. However, the structural remodeling of the RV, which plays a pivotal role in controlling the clinical course of PAH, has not been sufficiently studied from the metabolic perspective. Thus, performing the metabolomics analysis in these two important target organs of PAH may contribute to developing a thorough understanding of the mechanisms underlying flow-associated PAH pathogenesis. Meanwhile, the integrated analysis of shared dysregulated metabolites in PAs and the RV may be meaningful in elucidating the most significant metabolic feature of PAH and probably be helpful in exploiting potential therapeutic strategies for this devastating disease. Results of our current study suggest that the PAH pathogenesis could be mediated by widespread metabolic reprogramming, mainly including dysregulation of carbohydrate metabolism, lipid metabolism, and amino acid metabolism. Furthermore, in PAH rats, PAs and the RV share some common metabolic abnormalities, such as glycerophospholipid metabolism,

https://doi.org/10.1021/acsomega.1c05895
ACS Omega 2022, 7, 1273−1287

glycolysis/gluconeogenesis, linoleic acid metabolism, AA metabolism, and amino sugar and nucleotide sugar metabolism. In particular, the dysregulation of AA metabolism may considerably contribute to the development of flow-associated PAH.

EXPERIMENTAL SECTION

Animal Model of PAH and Grouping. All animal experiments were performed in accordance with the guideline of the Ministry of Health of the People's Republic of China and approved by the Animal Experimental Ethics Committee of the Guangxi Medical University. Sixteen male Sprague Dawley rats, purchased from the Animal Research Centre of the Guangxi Medical University, with weights ranging from 180 to 200 g, were randomly assigned into the following experimental groups: (1) the PAH group (n = 8), in which a model for flow-associated PAH was created by using the technique described in previous studies[67,68] with slight modifications. Briefly, PAH was established through combining subcutaneous injection of MCT (60 mg/kg, Sigma-Aldrich) with the aortocaval shunting procedure one week later (shunting surgery was carried out in accordance with our previous studies[69,70]); (2) the control group (n = 8) received saline injection (1 mL/rat, subcutaneously) and sham surgical operation (laparotomy) one week later. All experimental rats were raised under a 12:12 h light and dark cycle environment for four weeks after MCT/saline injection, freely accessing food and water.

Hemodynamic Measurement and RVH Assessment. Pentobarbital sodium (40 mg/kg intraperitoneally) was used to anesthetize experimental rats. The fistula and blood shunting between the abdominal aorta and the IVC were confirmed through two-dimensional and color Doppler ultrasonography. According to our previous studies,[69,71] through the right jugular vein, a cardiac catheter was inserted into the RV to monitor the pressure of the RV. Briefly, RVSP and RVMP were recorded by a transducer (BIOPAC Systems, Inc., Goleta, CA, USA). After the hemodynamic measurement, animals were sacrificed, and the heart and lungs were removed from the thorax. The RV-free wall was separated from the left ventricle (LV) and the septum (S) in cold phosphate-buffered saline (PBS), while PAs were separated from the lung tissue in cold PBS under a stereomicroscope. After separation, snap-frozen PAs (with liquid nitrogen) were transferred into a −80 °C freezer for LC−MS/MS analysis later, while the wet weight of the RV and the LV plus S was quickly measured. Next, half of the RV tissue was fixed in 4% paraformaldehyde, and the remaining half was snap-frozen and then kept in a −80 °C freezer for LC−MS/MS. The RVHI was calculated as a myocardial hypertrophy parameter according to the following formula: RVHI = RV/(LV + S).

Histological Analysis. After fixation with 4% paraformaldehyde for 24 h, the upper part of the left lung and half of the RV were subjected to paraffin embedding procedures; then, 5 μm-thick sections were prepared for histological examination. HE, GAF, and Masson's trichrome staining was conducted in accordance with the manufacturer's instructions to assess the morphology of pulmonary vessels and measure lung and heart collagen deposition. A video-linked microscope (Olympus, Fluoview1000, Japan) was used to obtain images of staining slides. At least three randomly selected pulmonary arterioles (outer diameter between 50 and 200 μm) per rat were assessed at 400 magnification to calculate the PAMT in accordance with the following formula: 100 × (external diameter − internal diameter)/external diameter.[72] The quantification of lung and RV collagen deposition was carried out by a pathologist who was unaware of the grouping of animals, using ImageJ version 2.1.0 software (NIH).

Sample Preparation for LC−MS/MS Analysis. Randomly selected PA (n = 4/group) and RV (n = 6/group) samples were collected for untargeted LC−MS/MS analysis. Briefly, PA and RV samples (100 mg) were homogenized in Milli-Q water (200 μL). Then, samples were mixed with 800 μL of methanol/acetonitrile solution (1:1 v/v) followed by vortexing and then sonicated at a low temperature. Next, samples were incubated for 1 h at −20 °C followed by centrifugation at 13,000 rpm for 15 min at 4 °C. After drying in a vacuum centrifuge, the supernatant was then stored at −80 °C prior to analysis. Before LC−MS/MS analysis, the supernatant of samples was redissolved in 100 μL of an acetonitrile/water (1:1 v/v) solvent. QC samples, which were prepared through mixing equal amounts (10 μL) of each sample together, were injected at a fixed interval and then analyzed with the same procedure as the experimental samples. LC−MS/MS was done at the Applied Protein Technology (APT, Shanghai).

Chromatographic Conditions of LC−MS/MS Analysis. LC−MS/MS analysis was performed on an Agilent, 1290 Infinity LC system (Agilent Technologies, Santa Clara, California, CA, United States) coupled with an AB SCIEX Triple TOF 6600 system (AB SCIEX, Framingham, MA, United States). A 2.1 mm × 100 mm ACQUITY UPLC BEH 1.7 μm amide column (130 Å, Waters, Ireland) was utilized to conduct chromatographic separation. The settings of the column were the following: temperature, 25 °C; injection volume, 2 μL; flow rate, 0.5 mL/min. The mobile phase of both ionization modes consisted of A, 25 mM ammonium acetate and 25 mM ammonium hydroxide in water, and B, acetonitrile. The gradient elution procedure was set as follows: 0−1 min, 85% B; 1−12 min, 85−65% B; 12−12.1 min, 65−40% B; 12.1−16.1 min, 40% B; 16.1−16.2 min, 40−85% B; 16.2−21.2 min, re-equilibration.

Mass Spectrometry Conditions of LC−MS/MS Analysis. The following are the settings of electrospray ionization source conditions: ion source (gas 1 and gas 2) pressure, 60 psi; curtain gas pressure, 30 psi; IonSpray Voltage Floating, ±5500 V; source temperature, 600 °C. The accumulation time for product ion scan was set at 0.05 s/spectrum. Information-dependent acquisition with high sensitivity mode was used to achieve the product ion scan. The following parameters were employed: collision energy, 35 V with ±15 eV; declustering potential, ±60 V; exclusion criteria for isotopes, within 4 Da; candidate ions to monitor per cycle, 10.

LC−MS/MS Data Processing and Analysis. ProteoWizard software version 3.0.6 was utilized to convert the LC−MS raw data into an MzXML format. Parameters on centWave employed for peak picking were the following: ppm = 25; peakwidth = c (10, 60); prefilter = c (10, 100). Moreover, the following parameters were employed for peak grouping: bw, 5; minfrac, 0.5; mzwid, 0.025. In the extracted ion features, only variables with more than 50% of the nonzero measurement values in at least one group were kept. Compound identification was carried out for metabolites through comparing the MS/MS spectra as well as the accurate m/z value (<25 ppm) to an in-house database, which was established with available authentic standards.

https://doi.org/10.1021/acsomega.1c05895
ACS Omega 2022, 7, 1273−1287

Umetrics SIMCA 14.1 (Umea, Sweden) was utilized to conduct multivariate data analysis, namely, PCA and OPLS-DA. The contribution of each variable to the classification was indicated by the VIP value that was calculated in the OPLS-DA model. The quality of the model was evaluated via seven-fold cross-validation and response permutation testing. The predictability and quality of the OPLS-DA model were assessed by utilizing Q^2 (cum) and R^2Y (cum) values, respectively. The Student's *t*-test at the univariate level was further employed to measure the significance of metabolites with VIP > 1.0. Metabolites with the *P*-value < 0.1 were considered as differential metabolites, while those with the *P*-value < 0.05 were recognized as statistically significant differential metabolites.[73] The heat map was generated via utilizing the package of pheatmap in the R platform (version 4.0.3). KEGG pathway analysis was conducted to investigate the metabolomic pathways involved in the pathogenesis of flow-associated PAH, by using the MetaboAnalyst 5.0 database. Data were uploaded to KEGG (www.kegg.jp) for more information and for drawing the dysregulated metabolic pathway networks.

Statistical Analysis. Data were presented as means ± SD and statistically analyzed with Prism 7 (GraphPad Software, Inc.). Statistically significant differences between two groups were determined via the Student's *t*-test. $P < 0.05$ was considered as a statistically significant difference.

■ ASSOCIATED CONTENT

Supporting Information

The Supporting Information is available free of charge at https://pubs.acs.org/doi/10.1021/acsomega.1c05895.

Detailed results of differential metabolites and dysregulated metabolic pathways in PAs and the RV in flow-associated PAH and list of abbreviations (PDF)

■ AUTHOR INFORMATION

Corresponding Author

Yusheng Pang − *Department of Pediatrics, The First Affiliated Hospital of Guangxi Medical University, Nanning 530021, China*; Email: pangyush@163.com

Authors

Dongli Liu − *Department of Pediatrics, The First Affiliated Hospital of Guangxi Medical University, Nanning 530021, China*; orcid.org/0000-0002-9316-5968

Suyuan Qin − *Department of Pediatrics, The First Affiliated Hospital of Guangxi Medical University, Nanning 530021, China*

Danyan Su − *Department of Pediatrics, The First Affiliated Hospital of Guangxi Medical University, Nanning 530021, China*

Kai Wang − *Department of Pediatrics, The First Affiliated Hospital of Guangxi Medical University, Nanning 530021, China; Department of Pediatrics, The First Affiliated Hospital of Wenzhou Medical University, Wenzhou 325015, China*

Yanyun Huang − *Department of Pediatrics, The First Affiliated Hospital of Guangxi Medical University, Nanning 530021, China*

Yuqin Huang − *Department of Pediatrics, The First Affiliated Hospital of Guangxi Medical University, Nanning 530021, China*

Complete contact information is available at: https://pubs.acs.org/10.1021/acsomega.1c05895

Notes

The authors declare no competing financial interest.

■ ACKNOWLEDGMENTS

This study was supported in part by the Natural Science Foundation of China (NSFC) (81660043), the Guangxi Medical University Youth Science Foundation (GXMUYSF202113), and the International Communication of Guangxi Medical University Graduate Education (2017). We acknowledge Shanghai Applied Protein Technology Co., Ltd. for providing LC−MS/MS analysis.

■ REFERENCES

(1) Alamri, A.; Burzangi, A. S.; Coats, P.; Watson, D. G. Untargeted Metabolic Profiling Cell-Based Approach of Pulmonary Artery Smooth Muscle Cells in Response to High Glucose and the Effect of the Antioxidant Vitamins D and E. *Metabolites* **2018**, *8*, 87.

(2) van de Veerdonk, M. C.; Kind, T.; Marcus, J. T.; Mauritz, G.-J.; Heymans, M. W.; Bogaard, H.-J.; Boonstra, A.; Marques, K. M. J.; Westerhof, N.; Vonk-Noordegraaf, A. Progressive right ventricular dysfunction in patients with pulmonary arterial hypertension responding to therapy. *J. Am. Coll. Cardiol.* **2011**, *58*, 2511−2519.

(3) Humbert, M.; Sitbon, O.; Chaouat, A.; Bertocchi, M.; Habib, G.; Gressin, V.; Yaïci, A.; Weitzenblum, E.; Cordier, J.-F.; Chabot, F.; et al. Survival in patients with idiopathic, familial, and anorexigen-associated pulmonary arterial hypertension in the modern management era. *Circulation* **2010**, *122*, 156−163.

(4) Rehman, J.; Archer, S. L. A proposed mitochondrial-metabolic mechanism for initiation and maintenance of pulmonary arterial hypertension in fawn-hooded rats: the Warburg model of pulmonary arterial hypertension. *Adv. Exp. Med. Biol.* **2010**, *661*, 171−185.

(5) Zhao, Y.; Peng, J.; Lu, C.; Hsin, M.; Mura, M.; Wu, L.; Chu, L.; Zamel, R.; Machuca, T.; Waddell, T.; et al. Metabolomic heterogeneity of pulmonary arterial hypertension. *PLoS One* **2014**, *9*, No. e88727. eCollection 2014

(6) Fessel, J. P.; Hamid, R.; Wittmann, B. M.; Robinson, L. J.; Blackwell, T.; Tada, Y.; Tanabe, N.; Tatsumi, K.; Hemnes, A. R.; West, J. D. Metabolomic analysis of bone morphogenetic protein receptor type 2 mutations in human pulmonary endothelium reveals widespread metabolic reprogramming. *Pulm. Circ.* **2012**, *2*, 201−213.

(7) Sutendra, G.; Bonnet, S.; Rochefort, G.; Haromy, A.; Folmes, K. D.; Lopaschuk, G. D.; Dyck, J. R.; Michelakis, E. D. Fatty acid oxidation and malonyl-CoA decarboxylase in the vascular remodeling of pulmonary hypertension. *Sci. Transl. Med.* **2010**, *2*, 44ra58.

(8) Hansmann, G.; Wagner, R. A.; Schellong, S.; Perez, V. A.; Urashima, T.; Wang, L.; Sheikh, A. Y.; Suen, R. S.; Stewart, D. J.; Rabinovitch, M. Pulmonary arterial hypertension is linked to insulin resistance and reversed by peroxisome proliferator-activated receptor-gamma activation. *Circulation* **2007**, *115*, 1275−1284.

(9) Tuder, R. M.; Davis, L. A.; Graham, B. B. Targeting energetic metabolism: a new frontier in the pathogenesis and treatment of pulmonary hypertension. *Am. J. Respir. Crit. Care Med.* **2012**, *185*, 260−266.

(10) Piao, L.; Marsboom, G.; Archer, S. L. Mitochondrial metabolic adaptation in right ventricular hypertrophy and failure. *J. Mol. Med.* **2010**, *88*, 1011−1020.

(11) Sutendra, G.; Michelakis, E. D. The metabolic basis of pulmonary arterial hypertension. *Cell Metab.* **2014**, *19*, 558−573.

(12) Paulin, R.; Michelakis, E. D. The metabolic theory of pulmonary arterial hypertension. *Circ. Res.* **2014**, *115*, 148−164.

(13) Arakaki, A. K.; Skolnick, J.; McDonald, J. F. Marker metabolites can be therapeutic targets as well. *Nature* **2008**, *456*, 443.

(14) Shao, F. J.; Ying, Y. T.; Tan, X.; Zhang, Q. Y.; Liao, W. T. Metabonomics Profiling Reveals Biochemical Pathways Associated

with Pulmonary Arterial Hypertension in Broiler Chickens. *J. Proteome Res.* **2018**, *17*, 3445−3453.
(15) Abd-Elsalam, W. H.; Alsherbiny, M. A.; Kung, J. Y.; Pate, D. W.; Löbenberg, R. LC-MS/MS quantitation of phytocannabinoids and their metabolites in biological matrices. *Talanta* **2019**, *204*, 846−867.
(16) Wang, X.; Shults, N. V.; Suzuki, Y. J. Oxidative profiling of the failing right heart in rats with pulmonary hypertension. *PLoS One* **2017**, *12*, No. e0176887.
(17) Xia, J.; Sinelnikov, I. V.; Han, B.; Wishart, D. S. MetaboAnalyst 3.0−making metabolomics more meaningful. *Nucleic Acids Res.* **2015**, *43*, W251−W257.
(18) Xia, J.; Wishart, D. S. MetPA: a web-based metabolomics tool for pathway analysis and visualization. *Bioinformatics* **2010**, *26*, 2342−2344.
(19) Pang, Z.; Chong, J.; Zhou, G.; de Lima Morais, D. A.; Chang, L.; Barrette, M.; Gauthier, C.; Jacques, P.; Li, S.; Xia, J. MetaboAnalyst 5.0: narrowing the gap between raw spectra and functional insights. *Nucleic Acids Res.* **2021**, *49*, W388−w396.
(20) Salmon, J. A.; Higgs, G. A. Prostaglandins and leukotrienes as inflammatory mediators. *Br. Med. Bull.* **1987**, *43*, 285−296.
(21) Urade, M. Cyclooxygenase (COX)-2 as a potent molecular target for prevention and therapy of oral cancer. *Jpn. Dent. Sci. Rev.* **2008**, *44*, 57−65.
(22) Stenmark, K. R.; James, S. L.; Voelkel, N. F.; Toews, W. H.; Reeves, J. T.; Murphy, R. C. Leukotriene C4 and D4 in neonates with hypoxemia and pulmonary hypertension. *N. Engl. J. Med.* **1983**, *309*, 77−80.
(23) Zheng, H. K.; Zhao, J. H.; Yan, Y.; Lian, T. Y.; Ye, J.; Wang, X. J.; Wang, Z.; Jing, Z. C.; He, Y. Y.; Yang, P. Metabolic reprogramming of the urea cycle pathway in experimental pulmonary arterial hypertension rats induced by monocrotaline. *Respir. Res.* **2018**, *19*, 94.
(24) Sakao, S.; Kawakami, E.; Shoji, H.; Naito, A.; Miwa, H.; Suda, R.; Sanada, T. J.; Tanabe, N.; Tatsumi, K. Metabolic remodeling in the right ventricle of rats with severe pulmonary arterial hypertension. *Mol. Med. Rep.* **2021**, *23*, 227.
(25) Chen, C.; Luo, F.; Wu, P.; Huang, Y.; Das, A.; Chen, S.; Chen, J.; Hu, X.; Li, F.; Fang, Z.; et al. Metabolomics reveals metabolite changes of patients with pulmonary arterial hypertension in China. *J. Cell Mol. Med.* **2020**, *24*, 2484−2496.
(26) Sanders, J. L.; Han, Y.; Urbina, M. F.; Systrom, D. M.; Waxman, A. B. Metabolomics of exercise pulmonary hypertension are intermediate between controls and patients with pulmonary arterial hypertension. *Pulm. Circ.* **2019**, *9*, 2045894019882623.
(27) Zhao, Y. D.; Chu, L.; Lin, K.; Granton, E.; Yin, L.; Peng, J.; Hsin, M.; Wu, L.; Yu, A.; Waddell, T.; et al. A Biochemical Approach to Understand the Pathogenesis of Advanced Pulmonary Arterial Hypertension: Metabolomic Profiles of Arginine, Sphingosine-1-Phosphate, and Heme of Human Lung. *PLoS One* **2015**, *10*, No. e0134958.
(28) Xu, W.; Comhair, S. A. A.; Chen, R.; Hu, B.; Hou, Y.; Zhou, Y.; Mavrakis, L. A.; Janocha, A. J.; Li, L.; Zhang, D.; et al. Integrative proteomics and phosphoproteomics in pulmonary arterial hypertension. *Sci. Rep.* **2019**, *9*, 18623.
(29) Izquierdo-Garcia, J. L.; Arias, T.; Rojas, Y.; Garcia-Ruiz, V.; Santos, A.; Martin-Puig, S.; Ruiz-Cabello, J. Metabolic Reprogramming in the Heart and Lung in a Murine Model of Pulmonary Arterial Hypertension. *Front. Cardiovasc. Med.* **2018**, *5*, 110.
(30) Zhao, J. H.; He, Y. Y.; Guo, S. S.; Yan, Y.; Wang, Z.; Ye, J.; Zhang, J. L.; Wang, Y.; Pang, X. B.; Xie, X. M.; et al. Circulating Plasma Metabolomic Profiles Differentiate Rodent Models of Pulmonary Hypertension and Idiopathic Pulmonary Arterial Hypertension Patients. *Am. J. Hypertens.* **2019**, *32*, 1109−1117.
(31) van Albada, M. E.; Schoemaker, R. G.; Kemna, M. S.; Cromme-Dijkhuis, A. H.; van Veghel, R.; Berger, R. M. The role of increased pulmonary blood flow in pulmonary arterial hypertension. *Eur. Respir. J.* **2005**, *26*, 487−493.
(32) van der Feen, D. E.; Bossers, G. P. L.; Hagdorn, Q. A. J.; Moonen, J. R.; Kurakula, K.; Szulcek, R.; Chappell, J.; Vallania, F.; Donato, M.; Kok, K.; et al. Cellular senescence impairs the reversibility of pulmonary arterial hypertension. *Sci. Transl. Med.* **2020**, *12*, No. eaaw4974.
(33) Rabinovitch, M.; Guignabert, C.; Humbert, M.; Nicolls, M. R. Inflammation and immunity in the pathogenesis of pulmonary arterial hypertension. *Circ. Res.* **2014**, *115*, 165−175.
(34) Hu, Y.; Chi, L.; Kuebler, W. M.; Goldenberg, N. M. Perivascular Inflammation in Pulmonary Arterial Hypertension. *Cell* **2020**, *9*, 2338.
(35) Stacher, E.; Graham, B. B.; Hunt, J. M.; Gandjeva, A.; Groshong, S. D.; McLaughlin, V. V.; Jessup, M.; Grizzle, W. E.; Aldred, M. A.; Cool, C. D.; et al. Modern age pathology of pulmonary arterial hypertension. *Am. J. Respir. Crit. Care Med.* **2012**, *186*, 261−272.
(36) Kominsky, D. J.; Campbell, E. L.; Colgan, S. P. Metabolic shifts in immunity and inflammation. *J. Immunol.* **2010**, *184*, 4062−4068.
(37) Zhang, C.; He, M.; Ni, L.; He, K.; Su, K.; Deng, Y.; Li, Y.; Xia, H. The Role of Arachidonic Acid Metabolism in Myocardial Ischemia-Reperfusion Injury. *Cell Biochem. Biophys.* **2020**, *78*, 255−265.
(38) Morin, C.; Hiram, R.; Rousseau, E.; Blier, P. U.; Fortin, S. Docosapentaenoic acid monoacylglyceride reduces inflammation and vascular remodeling in experimental pulmonary hypertension. *Am. J. Physiol.: Heart Circ. Physiol.* **2014**, *307*, H574−H586.
(39) Zhu, T.; Li, S.; Wang, J.; Liu, C.; Gao, L.; Zeng, Y.; Mao, R.; Cui, B.; Ji, H.; Chen, Z. Induced sputum metabolomic profiles and oxidative stress are associated with chronic obstructive pulmonary disease (COPD) severity: potential use for predictive, preventive, and personalized medicine. *EPMA J.* **2020**, *11*, 645−659.
(40) Dang, V. T.; Zhong, L. H.; Huang, A.; Deng, A.; Werstuck, G. H. Glycosphingolipids promote pro-atherogenic pathways in the pathogenesis of hyperglycemia-induced accelerated atherosclerosis. *Metabolomics* **2018**, *14*, 92.
(41) Cui, Y.; Liu, S.; Zhang, X.; Ding, X.; Duan, X.; Zhu, Z.; Zhang, J.; Liang, H.; Wang, D.; Zhang, G.; Yu, Z.; Yang, J.; Sun, T. Metabolomic Analysis of the Effects of Adipose-Derived Mesenchymal Stem Cell Treatment on Rats With Sepsis-Induced Acute Lung Injury. *Front. Pharmacol.* **2020**, *11*, 902.
(42) Bello-Klein, A.; Mancardi, D.; Araujo, A. S.; Schenkel, P. C.; Turck, P.; de Lima Seolin, B. G. Role of Redox Homeostasis and Inflammation in the Pathogenesis of Pulmonary Arterial Hypertension. *Curr. Med. Chem.* **2018**, *25*, 1340−1351.
(43) Schulze, P. C.; Drosatos, K.; Goldberg, I. J. Lipid Use and Misuse by the Heart. *Circ. Res.* **2016**, *118*, 1736−1751.
(44) Aragón-Herrera, A.; Feijóo-Bandín, S.; Otero Santiago, M.; Barral, L.; Campos-Toimil, M.; Gil-Longo, J.; Costa Pereira, T. M.; García-Caballero, T.; Rodríguez-Segade, S.; Rodríguez, J.; et al. Empagliflozin reduces the levels of CD36 and cardiotoxic lipids while improving autophagy in the hearts of Zucker diabetic fatty rats. *Biochem. Pharmacol.* **2019**, *170*, 113677.
(45) Wen, J.; Ma, X.; Niu, M.; Hao, J.; Huang, Y.; Wang, R.; Li, R.; Wang, J.; Zhao, Y. Metabolomics coupled with integrated approaches reveal the therapeutic effects of higenamine combined with [6]-gingerol on doxorubicin-induced chronic heart failure in rats. *Chin. Med.* **2020**, *15*, 120.
(46) Graham, B. B.; Kumar, R.; Mickael, C.; Kassa, B.; Koyanagi, D.; Sanders, L.; Zhang, L.; Perez, M.; Hernandez-Saavedra, D.; Valencia, C.; et al. Vascular Adaptation of the Right Ventricle in Experimental Pulmonary Hypertension. *Am. J. Respir. Cell Mol. Biol.* **2018**, *59*, 479−489.
(47) Liu, W.; Wei, Z.; Zhang, Y.; Liu, Y.; Bai, R.; Ma, C.; Yang, J.; Sun, D. Identification of three novel pathogenic mutations in sarcomere genes associated with familial hypertrophic cardiomyopathy based on multi-omics study. *Clin. Chim. Acta* **2021**, *520*, 43−52.
(48) Liu, X.; Zhang, Y.; Jiang, H.; Jiang, N.; Gao, J. Integrative analysis of the contribution of mRNAs and long non-coding RNAs to the pathogenesis of asthma. *Mol. Med. Rep.* **2019**, *20*, 2617−2624.
(49) Li, R.; Li, F.; Feng, Q.; Liu, Z.; Jie, Z.; Wen, B.; Xu, X.; Zhong, S.; Li, G.; He, K. An LC-MS based untargeted metabolomics study

https://doi.org/10.1021/acsomega.1c05895
ACS Omega 2022, 7, 1273−1287

identified novel biomarkers for coronary heart disease. *Mol. BioSyst.* **2016**, *12*, 3425−3434.
(50) Bujak, R.; Mateo, J.; Blanco, I.; Izquierdo-García, J. L.; Dudzik, D.; Markuszewski, M. J.; Peinado, V. I.; Laclaustra, M.; Barberá, J. A.; Barbas, C.; et al. New Biochemical Insights into the Mechanisms of Pulmonary Arterial Hypertension in Humans. *PLoS One* **2016**, *11*, No. e0160505.
(51) Ubhi, B. K.; Riley, J. H.; Shaw, P. A.; Lomas, D. A.; Tal-Singer, R.; MacNee, W.; Griffin, J. L.; Connor, S. C. Metabolic profiling detects biomarkers of protein degradation in COPD patients. *Eur. Respir. J.* **2012**, *40*, 345−355.
(52) Kaluarachchi, D. C.; Smith, C. J.; Klein, J. M.; Murray, J. C.; Dagle, J. M.; Ryckman, K. K. Polymorphisms in urea cycle enzyme genes are associated with persistent pulmonary hypertension of the newborn. *Pediatr. Res.* **2018**, *83*, 142−147.
(53) Würtz, P.; Havulinna, A. S.; Soininen, P.; Tynkkynen, T.; Prieto-Merino, D.; Tillin, T.; Ghorbani, A.; Artati, A.; Wang, Q.; Tiainen, M.; et al. Metabolite profiling and cardiovascular event risk: a prospective study of 3 population-based cohorts. *Circulation* **2015**, *131*, 774−785.
(54) Tan, R.; Li, J.; Liu, F.; Liao, P.; Ruiz, M.; Dupuis, J.; Zhu, L.; Hu, Q. Phenylalanine induces pulmonary hypertension through calcium-sensing receptor activation. *Am. J. Physiol.: Lung Cell. Mol. Physiol.* **2020**, *319*, L1010−l1020.
(55) MacLean, M. R. Pulmonary hypertension and the serotonin hypothesis: where are we now? *Int. J. Clin. Pract.* **2007**, 27−31.
(56) McGee, M.; Whitehead, N.; Martin, J.; Collins, N. Drug-associated pulmonary arterial hypertension. *Clin. Toxicol.* **2018**, *56*, 801−809.
(57) Simonneau, G.; Gatzoulis, M. A.; Adatia, I.; Celermajer, D.; Denton, C.; Ghofrani, A.; Gomez Sanchez, M. A.; Krishna Kumar, R.; Landzberg, M.; Machado, R. F.; et al. Updated clinical classification of pulmonary hypertension. *J. Am. Coll. Cardiol.* **2013**, *62*, D34−D41.
(58) Carubelli, V.; Castrini, A. I.; Lazzarini, V.; Gheorghiade, M.; Metra, M.; Lombardi, C. Amino acids and derivatives, a new treatment of chronic heart failure? *Heart Failure Rev.* **2015**, *20*, 39−51.
(59) DeBerardinis, R. J.; Mancuso, A.; Daikhin, E.; Nissim, I.; Yudkoff, M.; Wehrli, S.; Thompson, C. B. Beyond aerobic glycolysis: transformed cells can engage in glutamine metabolism that exceeds the requirement for protein and nucleotide synthesis. *Proc. Natl. Acad. Sci. U. S. A.* **2007**, *104*, 19345−19350.
(60) Sztormowska-Achranowicz, K.; Jankowski, Z.; Kocić, I. Protective effect of nicotinamide and L-arginine against monocrotaline-induced pulmonary hypertension in rats: gender dependence. *Pharmacol. Rep.* **2020**, *72*, 1334−1346.
(61) Smith, H. A.; Canter, J. A.; Christian, K. G.; Drinkwater, D. C.; Scholl, F. G.; Christman, B. W.; Rice, G. D.; Barr, F. E.; Summar, M. L. Nitric oxide precursors and congenital heart surgery: a randomized controlled trial of oral citrulline. *J. Thorac. Cardiovasc. Surg.* **2006**, *132*, 58−65.
(62) Orozco-Gutiérrez, J. J.; Castillo-Martínez, L.; Orea-Tejeda, A.; Vázquez-Díaz, O.; Valdespino-Trejo, A.; Narváez-David, R.; Keirns-Davis, C.; Carrasco-Ortiz, O.; Navarro-Navarro, A.; Sánchez-Santillán, R. Effect of L-arginine or L-citrulline oral supplementation on blood pressure and right ventricular function in heart failure patients with preserved ejection fraction. *Cardiol. J.* **2010**, *17*, 612−618.
(63) Lewis, G. D.; Ngo, D.; Hemnes, A. R.; Farrell, L.; Domos, C.; Pappagianopoulos, P. P.; Dhakal, B. P.; Souza, A.; Shi, X.; Pugh, M. E.; et al. Metabolic Profiling of Right Ventricular-Pulmonary Vascular Function Reveals Circulating Biomarkers of Pulmonary Hypertension. *J. Am. Coll. Cardiol.* **2016**, *67*, 174−189.
(64) Asnani, A.; Shi, X.; Farrell, L.; Lall, R.; Sebag, I. A.; Plana, J. C.; Gerszten, R. E.; Scherrer-Crosbie, M. Changes in Citric Acid Cycle and Nucleoside Metabolism Are Associated with Anthracycline Cardiotoxicity in Patients with Breast Cancer. *J. Cardiovasc. Transl. Res.* **2020**, *13*, 349−356.
(65) Assad, T. R.; Hemnes, A. R. Metabolic Dysfunction in Pulmonary Arterial Hypertension. *Curr. Hypertens. Rep.* **2015**, *17*, 20.
(66) Prisco, S. Z.; Eklund, M.; Moutsoglou, D. M.; Prisco, A. R.; Khoruts, A.; Weir, E. K.; Thenappan, T.; Prins, K. W. Intermittent Fasting Enhances Right Ventricular Function in Preclinical Pulmonary Arterial Hypertension. *J. Am. Heart Assoc.* **2021**, *10*, No. e022722.
(67) Bartelds, B.; van Loon, R. L. E.; Mohaupt, S.; Wijnberg, H.; Dickinson, M. G.; Boersma, B.; Takens, J.; van Albada, M.; Berger, R. M. F. Mast cell inhibition improves pulmonary vascular remodeling in pulmonary hypertension. *Chest* **2012**, *141*, 651−660.
(68) Borgdorff, M. A.; Bartelds, B.; Dickinson, M. G.; Steendijk, P.; de Vroomen, M.; Berger, R. M. Distinct loading conditions reveal various patterns of right ventricular adaptation. *Am. J. Physiol.: Heart Circ. Physiol.* **2013**, *305*, H354−H364.
(69) Shang, L.; Wang, K.; Liu, D.; Qin, S.; Huang, J.; Zhao, Y.; Pang, Y. TMEM16A regulates the cell cycle of pulmonary artery smooth muscle cells in high-flow-induced pulmonary arterial hypertension rat model. *Exp. Ther. Med.* **2020**, *19*, 3275−3281.
(70) Liu, D.; Wang, K.; Su, D.; Huang, Y.; Shang, L.; Zhao, Y.; Huang, J.; Pang, Y. TMEM16A Regulates Pulmonary Arterial Smooth Muscle Cells Proliferation via p38MAPK/ERK Pathway in High Pulmonary Blood Flow-Induced Pulmonary Arterial Hypertension. *J. Vasc. Res.* **2020**, *58*, 27−37.
(71) Wang, K.; Chen, C.; Ma, J.; Lao, J.; Pang, Y. Contribution of calcium-activated chloride channel to elevated pulmonary artery pressure in pulmonary arterial hypertension induced by high pulmonary blood flow. *Int. J. Clin. Exp. Pathol.* **2015**, *8*, 146−154.
(72) Nawa, N.; Ishida, H.; Katsuragi, S.; Baden, H.; Takahashi, K.; Higeno, R.; Torigoe, F.; Mihara, S.; Narita, J.; Miura, K.; et al. Constitutively active form of natriuretic peptide receptor 2 ameliorates experimental pulmonary arterial hypertension. *Mol. Ther.–Methods Clin. Dev.* **2016**, *3*, 16044.
(73) Luo, D.; Deng, T.; Yuan, W.; Deng, H.; Jin, M. Plasma metabolomic study in Chinese patients with wet age-related macular degeneration. *BMC Ophthalmol.* **2017**, *17*, 165.

https://doi.org/10.1021/acsomega.1c05895
ACS Omega 2022, 7, 1273−1287